Computer Methods and Programs in Biomedicine 204 (2021) 106062

Contents lists available at ScienceDirect

Computer Methods and Programs in Biomedicine

journal homepage: www.elsevier.com/locate/cmpb

Tube-load model: A clinically applicable pulse contour analysis method for estimation of cardiac stroke volume

Rachel Smith[a,*], Liam Murphy[a], Christopher G. Pretty[a], Thomas Desaive[b], Geoffrey M. Shaw[c], J. Geoffrey Chase[a]

[a] Department of Mechanical Engineering, University of Canterbury, New Zealand
[b] IGA Cardiovascular Science, University of Liége, Liége, Belgium
[c] Christchurch Hospital Intensive Care Unit, New Zealand

ARTICLE INFO

Article history:
Received 8 February 2021
Accepted 17 March 2021

Keywords:
Pulse contour analysis
Tube-load model
Stroke volume
Hemodynamic monitoring
Intensive care
Arterial wave reflection

ABSTRACT

Background and Objectives: Accurate, reproducible, and reliable real-time clinical measurement of stroke volume (SV) is challenging. To accurately estimate arterial mechanics and SV by pulse contour analysis, accounting for wave reflection, such as by a tube-load model, is potentially important. This study tests for the first time whether a dynamically identified tube-load model, given a single peripheral arterial input signal and pulse transit time (PTT), provides accurate SV estimates during hemodynamic instability.

Methods: The model is tested for 5 pigs during hemodynamic interventions, using either an aortic flow probe or admittance catheter for a validation SV measure. Performance is assessed using Bland-Altman and polar plot analysis for a series of long-term state-change and short-term dynamic events.

Results: The overall median bias and limits of agreement (2.5th, 97.5th percentile) from Bland-Altman analysis were -10% [-49, 36], and -1% [-28,20] for state-change and dynamic events, respectively. The angular limit of agreement (maximum of 2.5th, 97.5th percentile) from polar-plot analysis for state-change and dynamic interventions was 35.6°, and 35.2°, respectively.

Conclusion: SV estimation agreement and trending performance was reasonable given the severity of the interventions. This simple yet robust method has potential to track SV within acceptable limits during hemodynamic instability in critically ill patients, provided a sufficiently accurate PTT measure.

1. Introduction

Stroke volume (SV) and cardiac output (CO) are important clinical metrics for hemodynamic management of critically ill patients, particularly for diagnosing and managing circulatory failure [1–3] a major contributor to mortality in intensive care unit (ICU) [4]. SV and CO provide information on blood flow out of the heart beat-by-beat and on average, respectively. The European Society of Intensive Care Medicine has recommended using these metrics, measured in real-time, to evaluate patient status and response to therapy [5].

However, accurate real-time clinical measurement of SV and CO is challenging. Indicator dilution, the clinical gold standard CO monitoring method, is invasive, intensive [3,6], and adds fluid load. Pulse contour analysis methods use only an arterial waveform to estimate CO, while being non-additionally invasive. However, current, clinically available, non-additionally invasive devices have insufficient accuracy for use in critically ill patients [6]. Further work is needed to develop non-additionally invasive monitoring for SV or CO, which is reproducible and reliable across a range of physiological states [7,8].

Existing pulse contour analysis devices use features of the arterial waveform [6] (e.g. standard deviation, area under the systolic portion of the curve) or more complex mathematical models based on waveform shape (e.g. the 3-Element Windkessel model [9,10]). However, these methods generally cannot account for wave reflection in the arterial system, where a pressure wave travelling away from the heart is reflected backwards due to impedance differences in the arteries, such as at bifurcations [11]. These reflected waves alter the shape of arterial flow and pressure waveforms [11]. Thus, accounting for wave reflection is potentially important for determining arterial pressure-flow relationships to accurately estimate arterial mechanics and, subsequently, SV / CO by pulse contour analysis.

* Corresponding author.
E-mail address: rachel.smith@pg.canterbury.ac.nz (R. Smith).

https://doi.org/10.1016/j.cmpb.2021.106062
0169-2607/

Tube-load models capture wave propagation and reflection phenomena, with the benefit of few parameters [12], so they are clinically identifiable. A review of tube-load models for monitoring arterial hemodynamics is given in [12]. Generally, model usage focuses on monitoring central pressures from peripheral ones, and investigating various phenomena including wave reflection and compliance. Hahn et al. [13] use 2 distinct peripheral arterial pressure waveforms to estimate central pressure and flow using a tube-load model, although SV / CO estimation accuracy is not directly investigated. Some preliminary studies investigate tube-load / transfer function based models to identify CO with clinically acceptable outcome, using carotid and femoral arterial pressures [14,15].

This study tests whether a dynamically identified tube-load model given a clinically common, single peripheral arterial input signal, and pulse transit time (PTT) provides a sufficiently accurate estimate of SV during hemodynamic instability. A novel method for using the tube-load model for pulse contour analysis to obtain non-additionally-invasive, continuous, model-based SV estimation is presented. SV monitoring meeting this description would enable direct monitoring of heart function and response to care with insight and resolution not currently possible [16].

2. Materials and methods

2.1. Porcine trials and measurements

5 pure Piétrain pigs, weighing 18.5kg to 29.0kg, were used. Initial sedation and anaesthesia was achieved using Zoletil (0.1mLkg^{-1}) and diazepam (1mg kg^{-1}). A continuous infusion of sufentanil (0.1mL kg^{-1} at 0.005mg mL^{-1}), Thiobarbital (0.1mL kg^{-1}h^{-1}) and Nimbex (1mL kg^{-1}h^{-1} at 2mg mL^{-1}), delivered via superior vena cava catheter were used to maintain sedation and anesthesia. Pigs were mechanically ventilated via tracheostomy, using a GE Engstrom CareStation mechanical ventilator (GE 92 Healthcare, Waukesha, US) with baseline positive end-expiratory pressure (PEEP) of 5 cmH_2O and tidal volume of 10mL kg^{-}1.

Left ventricular pressures and volumes (V_{LV}) were measured using 7F micromanometer-tipped admittance catheters (Transonic Scisense Inc., Ontario, Canada). Blood pressure was measured using high fidelity pressure catheters (Transonic, Ithaca, NY, USA) in the proximal aorta (P_{ao}) and femoral artery (P_{fem}). Aortic flow (Q_{ao}) was measured from an aortic flow probe positioned on the proximal aorta near the aortic valve (Transonic, Ithaca, NY, USA). Once the probe was located, the thorax was held closed using clamps. All data was recorded as a single Notocord data file (Instem, Croissy-sur-Seine, France), at a sampling rate of 250Hz.

Pigs underwent several interventions: a respiratory recruitment manouevre (RM) in which PEEP is increased in steps of 5 cmH_2O to PEEP of $\geq$ 15 cmH_2O to reduce systemic venous return and thus SV [2]; a fluid infusion of 500mL of saline solution over30min to increase circulatory volume and ventricular preload; and an infusion of E. Coli lipopolysaccharide (0.5mg kg^{-}1 over 30minute) to produce a septic shock like response [17].

Pig experiments were conducted at the Centre Hospitalier Universitaire de Liége, Belgium and were approved by the Ethics Committee of the University of Li**é**ge Medical Faculty, permit number 14–1726.

2.2. Data collection

State-change events, 5 short periods with a duration of 10 beats to test the ability of the model to track longer-term changes between a range of hemodynamic states, were identified and analysed:

1. *Control:* At the beginning of the experiment, after instrumentation is in place, and the pig is in a stable state.
2. *high PEEP:* During high PEEP ($\geq$ 15 cmH_2O) of a recruitment manoeuvre.
3. *high Fluids:* Shortly following the end of the fluid infusion intervention.
4. *Start Endotoxin:* During start of the endotoxin infusion.
5. *End Endotoxin:* Just prior to the end of the endotoxin infusion, or just prior to circulatory failure in pigs 1, 3, & 5 for which cardiac failure occurred before completion of the full 30 minute infusion.

For these events, the model is calibrated during the control event and SV estimation accuracy is assessed for subsequent interventions periods, matching potential clinical use.

Dynamic Events, two longer events to assess the ability of the model to track rapid SV changes during hemodynamic instability, were identified and analysed for each pig:

1. *RM:* 8 minutes encompassing a recruitment manoeuvre, prior to fluid / endotoxin infusions.
2. *Endotoxin:* The final 8 minutes of the 30 minute endotoxin infusion for pigs 2 & 4, or the final 8 minutes up until circulatory failure for Pigs 1, 3, & 5.

For these events, the model is calibrated during the first 10 beats of the event, and SV estimation accuracy is assessed for all subsequent beats. The fluid infusion intervention is not used because SV remained stable in most pigs. The experimental time-schedule and events are illustrated in Fig 1.

2.3. Signal processing and beat identification

All signals were filtered with a 5th order Butterworth low-pass filter, with a cut-off frequency of 20 Hz (P_{fem}, P_{ao}) and 10 Hz for noisier signals (V_{LV}, Q_{ao}). Filtered waveforms were used for all subsequent analysis.

The foot (t_0) of each waveform (P_{fem}, P_{ao}, Q_{ao}), marking the beginning of systole / contraction was found using a shear-transform algorithm [18]. The end-systole point (t_d) for P_{fem} & P_{ao}, marking the end of contraction, was identified using a second-derivative based method [19]. *PTT* was identified as the time delay between the foot of P_{ao} ($t_{0,ao}$) and P_{fem} ($t_{0,fem}$), providing an accurate measure of *PTT* for model validation. Less invasive estimates of *PTT* could be obtained via various clinically available devices [20] as invasive aortic catheterization is clinically infeasible.

2.4. Validation SV measure

Measured SV (SV_{mea}) is used for validation and calibration as measured from integrating an aortic flow probe signal (Q_{ao}) in Pigs 2 - 5. For Pig 1 an admittance catheter was used due to sensor error from the aortic flow probe. In this case, SV_{mea} was calculated as the difference between the maximum and minimum ventricle volume (V_{LV}) for each beat.

2.5. Pulse contour analysis method

The tube-load model describes the arterial system as an arbitrary number of parallel uniform lossless tubes, representing the large conduit arteries, in series with loads, representing peripheral blood vessels [12], as shown in Fig 2. Pressure waves generated by the heart travel through the large arteries to the periphery over a the pulse transit time (*PTT*). Some component of these forward-travelling waves is reflected, creating backward waves, which lead to differences between Q_{ao} and P_{ao} waveform shapes as pressure waves add whereas flow waves subtract [11]. The tube-load model

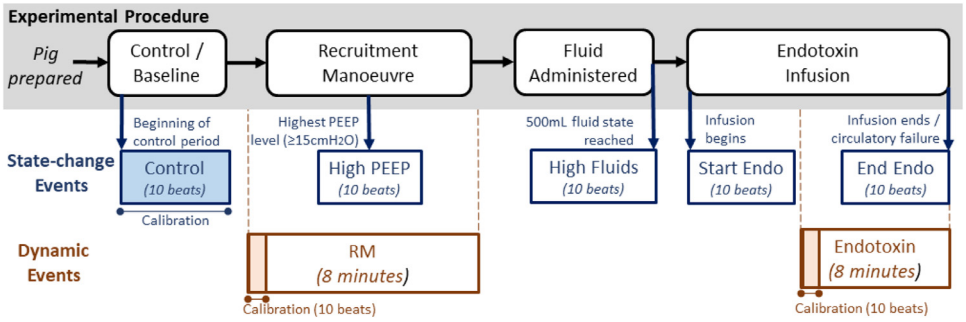

Fig. 1. Time-schedule of experimental procedure and data collected. 5 state-change events and 2 dynamic events test model SV estimation accuracy across hemodynamic states, and during rapid changes, respectively.

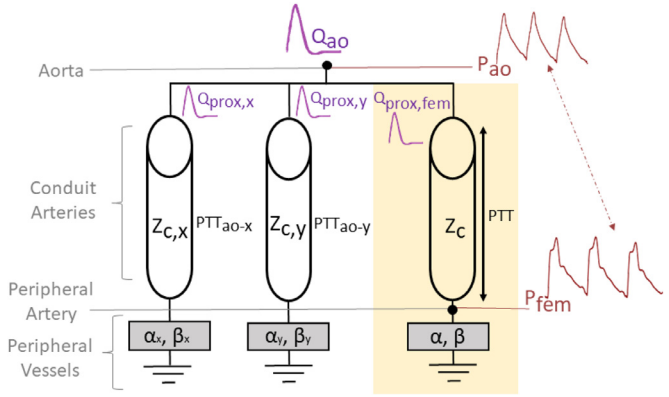

Fig. 2. Tube-load model schematic. The arterial system is modelled as an arbitrary number of parallel tubes, representing conduit arteries, in series with a load, representing peripheral vessels. Each pathway is characterized by 4 values (PTT, Z_c, α, and β).

captures this effect by modelling wave propagation forwards and backwards along the uniform tubes.

Each tube and load represents a pathway to a different peripheral vascular bed. In this model, pressure at the proximal end of each tube is equal to P_{ao} (i.e. $P_{ao} = P_{x,prox} = P_{y,prox}$). Q_{ao} is equal to the sum of the proximal flows for all tubes (i.e $Q_{ao} = \sum Q_{prox,i} = Q_{ao,a} + Q_{ao,b} + \ldots$) [12].

The aorta-femoral artery pathway is modelled as one tube & load, and measured P_{fem} & PTT are used to estimate central flows ($Q_{ao,est}$), assuming changes in $Q_{prox,fem}$ are representative of changes in Q_{ao}. Characteristic impedance of the tube (Z_c), representing resistance of the conduit arteries, is assumed constant. Impedance of distal arterial beds (Z_{load}) is modelled in the frequency domain as a single pole and zero, characterized by parameters A, B, with a gain factor Z_c:

$$Z_{load}(\omega) = Z_c \frac{j\omega + B}{j\omega + A} \tag{1}$$

where $(0 < A < B)$ and Z_c is the impedance of the corresponding tube, ensuring pressure wave reflections are positive, stable, and become negligible at high frequencies [21]. As ω becomes very large, the peripheral load tends to Z_c and the tube and load are impedance matched, so there are no reflections.

The model can be used to create transfer functions between central and peripheral pressures and flows in the frequency domain. Thus, $P_{ao,est}$, and $Q_{ao,est}$ are calculated using measured P_{fem} & PTT:

$$\frac{P_{ao,est}(\omega)}{P_{fem}(\omega)} = \frac{(\frac{B+A}{2} + j\omega)e^{j\omega PTT} + (\frac{B-A}{2})e^{-j\omega PTT}}{j\omega + B} \tag{2}$$

$$\frac{ZQ_{ao,est}(\omega)}{P_{fem}(\omega)} = \frac{(\frac{B+A}{2} + j\omega)e^{j\omega PTT} - (\frac{B-A}{2})e^{-j\omega PTT}}{j\omega + B} \tag{3}$$

where $ZQ_{ao,est} = Q_{prox,fem} \times Z_c \times C$. The component of aortic flow corresponding to the femoral artery pathway is $Q_{prox,fem}$ [12]. This model assumes $Q_{prox,fem}$ is representative of the total aortic flow Q_{ao}, and can be scaled by a factor C to obtain $Q_{ao,est}$. Z thus incorporates both the characteristic impedance of the tube Z_c and this scale factor C.

Using a Laplace transform and discretization (derivation provided in Appendix A), these equations can be represented in the time domain:

$$P_{ao,est}[n] = \alpha P_{ao,est}[n-1] + \beta P_{fem}[n + PTT \cdot F_s] - \alpha P_{fem}[n + PTT \cdot F_s - 1] + (1-\beta)P_{fem}[n - PTT \cdot F_s] \tag{4}$$

$$ZQ_{ao,est}[n] = \alpha Q_{ao,est}[n-1] + \beta P_{fem}[n + PTT \cdot F_s] - \alpha P_{fem}[n + PTT \cdot F_s - 1] - (1-\beta)P_{fem}[n - PTT \cdot F_s] \tag{5}$$

where F_s is the sampling frequency of the signal, and α, β are unitless, new parameters representing distal arterial properties (derived in Appendix A), with a range of $(0 < \alpha < \beta \leq 1)$.

Hence, knowing P_{fem} we can estimate arterial flow $Q_{ao,est}$, given model parameters (α, β, Z).

2.6. Identification of model parameters

Distal arterial properties (α, β) are identified by optimizing two error criteria, similar to [21,22]. Prior knowledge of Q_{ao} and P_{ao} shapes are used in defining the error criteria to identify optimal parameters:

- $P_{ao,est}$ has an exponential decay during diastole to be physiologically realistic [11]. Thus, during diastole, $ln(P_{ao,est}(t))$ is approximately linear. A linear regression line of best fit $(L(t))$ of each beats' diastolic period was calculated from $ln(P_{ao,est}(t))$ during diastole. This linear fit was used to define the P_{ao} component of the error using the difference between the $P_{ao,est,diastole}$ and the best-fit exponential decay: $E_{P_{ao}} = Mean|P_{ao,est,diastole}(t) - e^{L(t)}|$.
- Flow in the aorta is zero during diastole, as the aortic valve is closed (i.e. $ZQ_{ao,est}(t) \approx 0$). The $ZQ_{ao,est}$ waveform, calculated from Eq. 5, subsequently has its mean diastolic value subtracted, so average diastolic flow is zero. The Q_{ao} component of the error is then calculated using the difference between $ZQ_{ao,est,diastole}$ and 0: $E_{Q_{ao}} = Mean|ZQ_{ao,est,diastole-0}|$
- For non-control events it is assumed parameters should be similar to control identified values. Thus, the error distribution $E(\alpha, \beta)$ is weighted by the error distribution from control

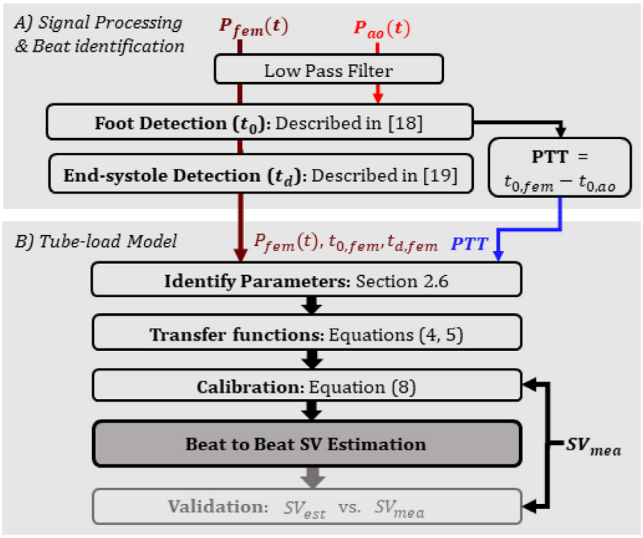

Fig. 3. Summary of steps for tube-load model computational method. A) Signal processing and beat identification: P_{fem} & P_{ao} are filtered. The foot (t_0) of each signal is identified and used for PTT calculation. End-systole time (t_d) is calculated for P_{fem}. B) Tube-load model: P_{fem} & PTT are inputs to the model. SV_{mea} is required for a short calibration period. The model provides beat to beat SV estimates (SV_{est}) subsequent to calibration. SV_{mea} is used to validate SV_{est}.

which favors control parameter values. This choice aims to reduce 'random' parameter fluctuations from control, but still allow parameters to evolve.

These errors are combined for non-control events:

$$E(\alpha,\beta) = \sqrt{(E_{P_{ao}}(\alpha,\beta) \times E_{Q_{ao}}(\alpha,\beta)) \times E_{control}(\alpha,\beta)} \quad (6)$$

For control events the error is simply $E_{P_{ao}} \times E_{Q_{ao}}$.

α, β corresponding the lowest error were identified using a grid search for parameters $\frac{\alpha}{\beta}$, β over their full range of 0–1. For state-change events, parameters are identified once for each event, minimising error across all 10 beats. For dynamic events, parameters are calculated each beat. In this case, error was minimised for waveforms over a 9 beat window centered on the given beat, to smooth measurement noise effects.

Having identified α & β, $P_{ao,est}$ & $ZQ_{ao,est}$ are calculated using Eqs. 4 and 5, respectively. Waveforms were calculated for each beat individually for dynamic events, and for all beats simultaneously for state-change events.

Calibration Factor (Z) is a fixed parameter, identified during calibration. It bundles $Z_c \times C$. Z_c is fixed, and thus assumes the large conduit arteries modelled by this parameter have negligible change in vascular tone [11]. C is the proportion of aortic flow travelling to the femoral artery, assumed to be constant on the basis the

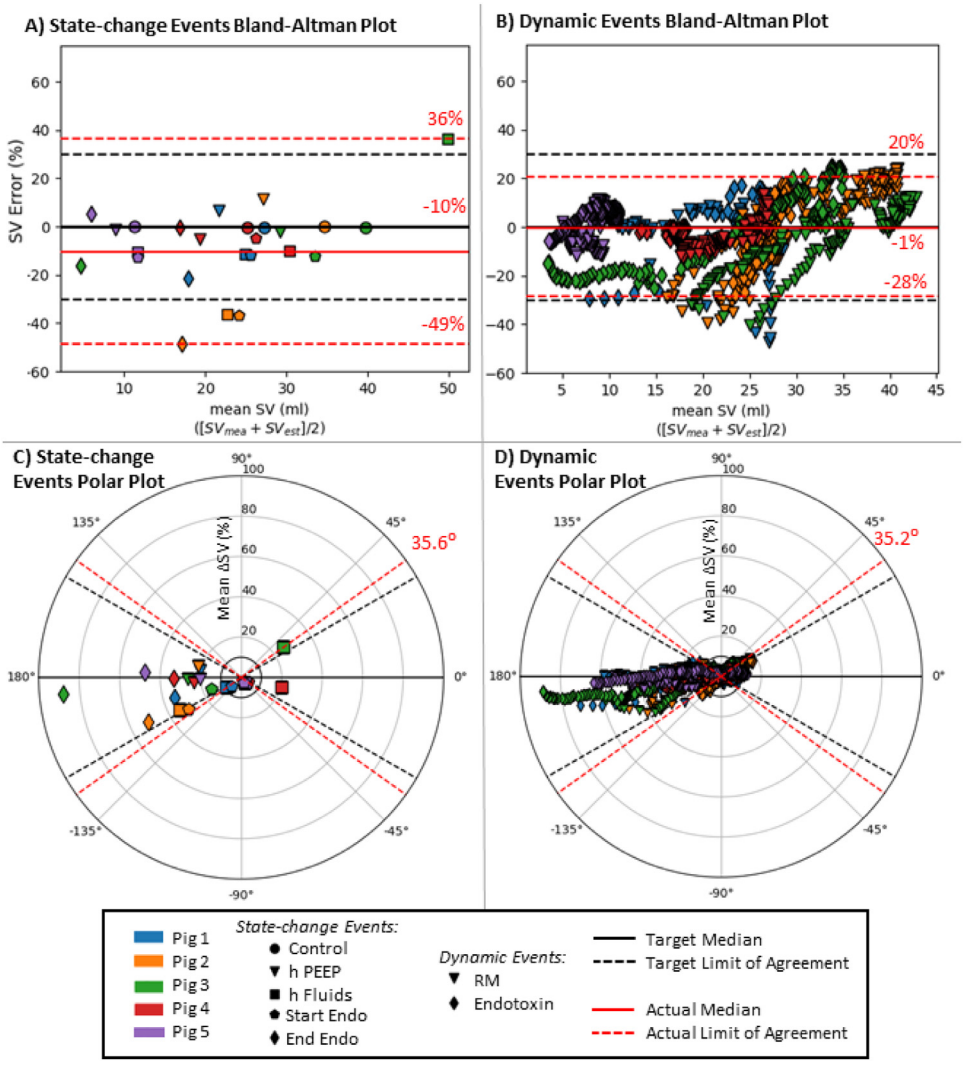

Fig. 4. Bland-Altman analysis for A) state-change events, B) dynamic events. Polar plot analysis for C) state-change events, D) dynamic events. Target and actual median bias are shown, as well as limits of agreement. For clarity every 4th beat is plotted in B, D, but all beats are used in bias / limits of agreement calculation.

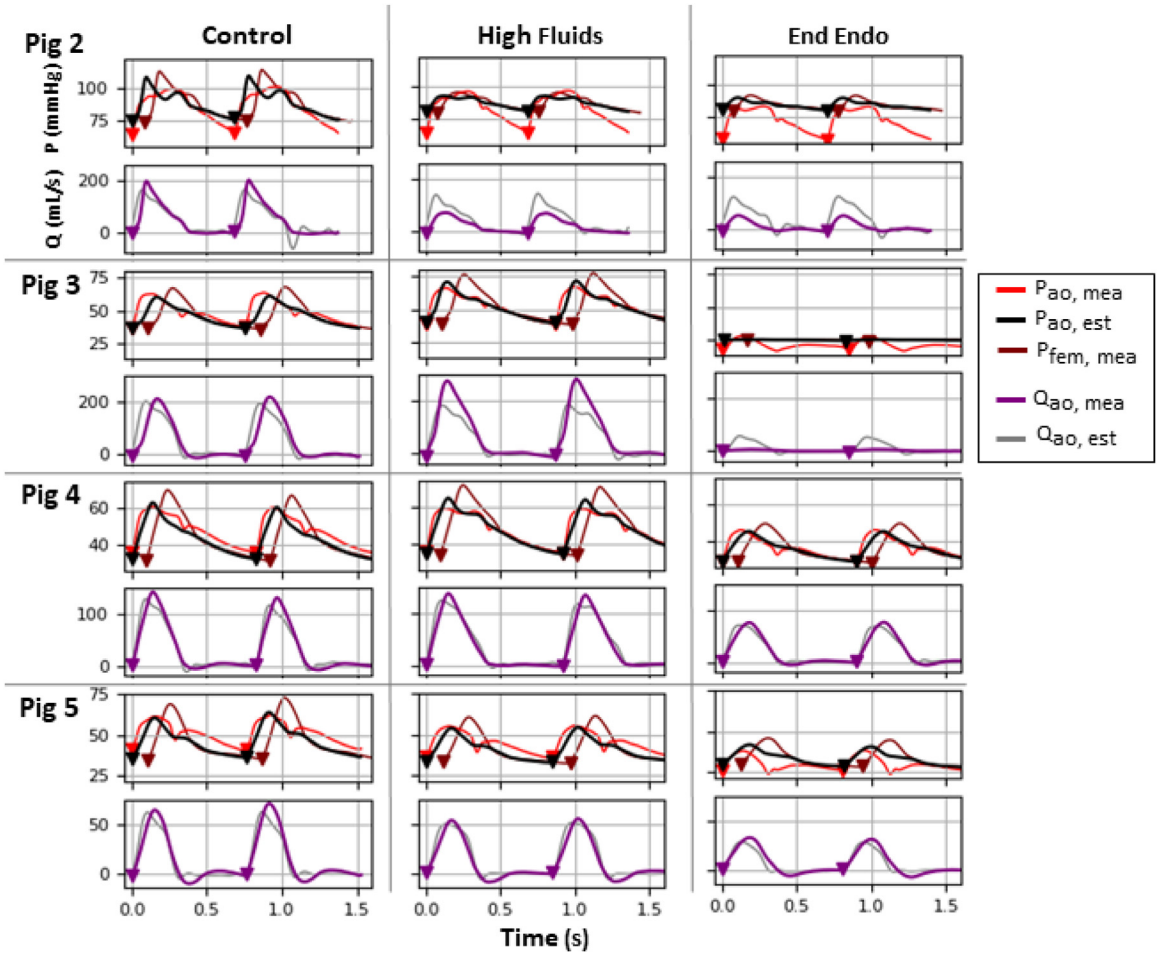

Fig. 5. Example $P_{ao,est}$ & $Q_{ao,est}$ waveforms from model transfer functions (Eqs. 4, 5, respectively) for Pigs 2–5 (all with $Q_{ao,mea}$) from 3 state-change events. Markers indicate the foot (t_0) of each waveform.

femoral artery is a relatively major artery, the largest used for routine catheter placement [23].

2.7. Model calibration

Model SV estimates were calibrated from SV_{mea}. In a clinical setting, the model could be calibrated using a non-invasive SV metric, such as echocardiography [24]. The calibration period was the control event of the state-change events, and first 10 beats of each dynamic event, as detailed in Fig 1. The value of Z identified during control was used for all subsequent events for state-change events. For dynamic events, Z was used for all subsequent beats of the specific event.

From the control period, z_n, was calculated beat-wise for the n^{th} beat using SV_{mea}, by enforcing:

$$SV_{mea,\,n} = SV_{est,\,n} = \frac{1}{Z}\int_{t_{0,n}}^{t_{0,n+1}} ZQ_{ao,est}(\tau)\,d\tau \tag{7}$$

And thus z_n for that beat can be identified from:

$$z_n = \frac{1}{SV_{mea,\,n}}\int_{t_{0,n}}^{t_{0,n+1}} ZQ_{ao,est}(\tau)\,d\tau \tag{8}$$

where z_n values for all 10 control beats are averaged to reduce the impact of measurement noise, obtaining a single calibration value Z.

Having identified all model parameters and calibrated the model, SV_{est} is calculated as the area under $Q_{ao,est}$.

The steps for this computational method are summarised in Fig 3.

2.8. Analysis

For state-change events, SV error and ΔSV were calculated for each event subsequent to control (shown in Fig 1), to assess the agreement and trending ability of the model.

SV error for a given event is calculated as a percentage of control SV: $Error_{event} = (\overline{SV}_{est,event} - \overline{SV}_{mea,event})/\overline{SV}_{mea,control} \times 100\%$. This calculation of error is useful because its magnitude is relative to SV during baseline state. It avoids the numerical issues where, during extreme circulatory failure, SV is very small, meaning errors of only a few ml yield very high percentage error.

ΔSV was calculated each event to find ΔSV_{mea} and ΔSV_{est} using: $\Delta SV = (\overline{SV}_{event} - \overline{SV}_{control})/\overline{SV}_{control} \times 100\%$.

For dynamic events, a 10-beat moving average of SV (SV_{filt}) is calculated and used to calculate SV error and ΔSV. This approach avoids large irregular SV fluctuations during periods of arrhythmia, and regular stroke volume variation (SVV) over the respiratory cycle [25] from obscuring SV changes in response to each intervention. Fig. 1 shows the two interventions and 10 control beats used each time.

Bland-Altman analysis is used to assess the agreement between SV_{mea} and SV_{est} [26]. The median bias and 95% range [2.5th, 97.5th percentiles] is used for limits of agreement, ensuring no assumption is made about how error is distributed. Critchley & Critchley propose acceptable limits of agreement of ±30% [27] and Peyton &

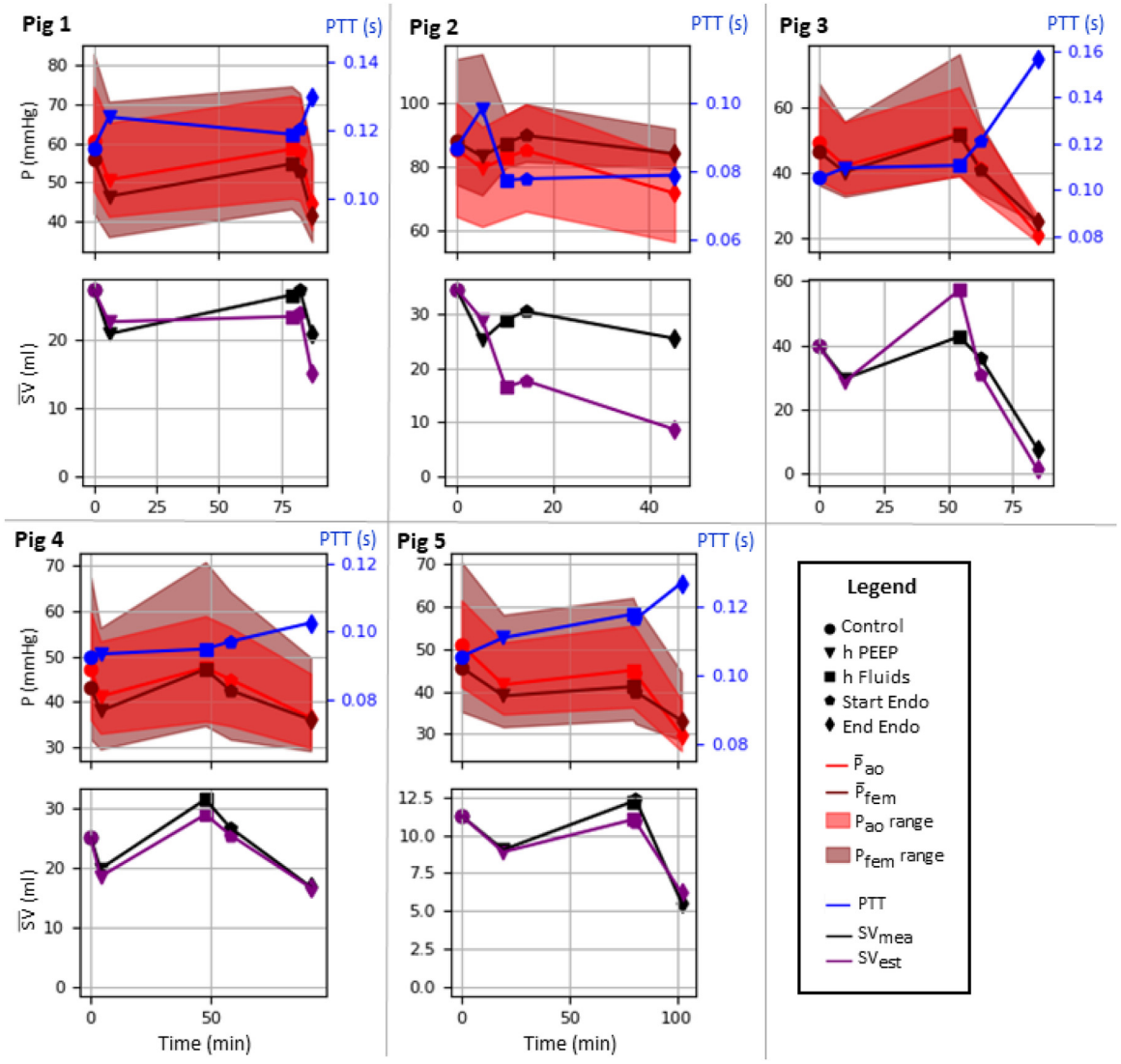

Fig. 6. Pressures, PTT, and SV across state-change events for each pig. Mean pressures for each event are plotted as a line, with the mean range (foot-peak) shaded.

Chong propose acceptable limits of ±45% [28]. This study uses the more conservative 30% limits.

Polar plot analysis is used to assess the trending ability of the proposed method[29]. For each SV measurement an X-Y pair of ΔSV is calculated (X: ΔSV_{mea}, Y: ΔSV_{est}). Polar angle (θ) is calculated as the angle of divergence of the ΔSV X-Y vector from the identity line Y=X. Radius is the mean ΔSV of the two methods.

Trending ability was assessed using angular limits of agreement, defined as the larger value of the 2.5th & 97.5th percentile of θ, calculated with angles converted to -90° - 90°. Only sufficiently large ΔSV are used in calculating limits of agreement, with changes within a radius < 10% being ignored, as suggested in [29]. The acceptable angular limits of agreement used are ±30° as proposed by Critchley [29].

3. Results

The results of Bland-Altman and polar plot analysis are shown in Fig 4. Bland-Altman plots show agreement of SV_{mea} and SV_{est} outside acceptable limits for state-change events (A), with high errors for 4 interventions, and inside acceptable limits for dynamic events (B). Polar plots show trending ability almost within acceptable limits for both state-change (C) and dynamic events (D), with ΔSVs close to an angle of zero, and limits of radial agreement near to 30°. Most errors are on the lower left side of the polar plot, reflecting interventions leading to negative ΔSVs, with the model overestimating SV reductions.

Fig 5 shows the physiologically realistic central arterial pressure and flow waveforms delivered by the model. Fig 6 shows changes in average arterial pressures, PTT, SV_{mea} and SV_{est} across state-change events, for each pig. Fig 7 shows the equivalent for dynamic events. These figures show, in most pigs, SV_{est} followed a similar trend to SV_{mea}. Summary tables of measured arterial pressures, PTT, and SV are provided in Appendix B.

4. Discussion

4.1. Response to interventions

The experimental protocol provided a range of hemodynamic states to test the model. State-change events provided a range of SVs, spread across 1 - 2 hours (SVs shown in Fig 6), providing a way to test model accuracy for changes in state over time. The dynamic events provided rapid SV changes over 8 min, testing the ability to capture rapid changes and beat-beat function (SVs shown in Fig 7). In particular, the endotoxin infusion led to circulatory

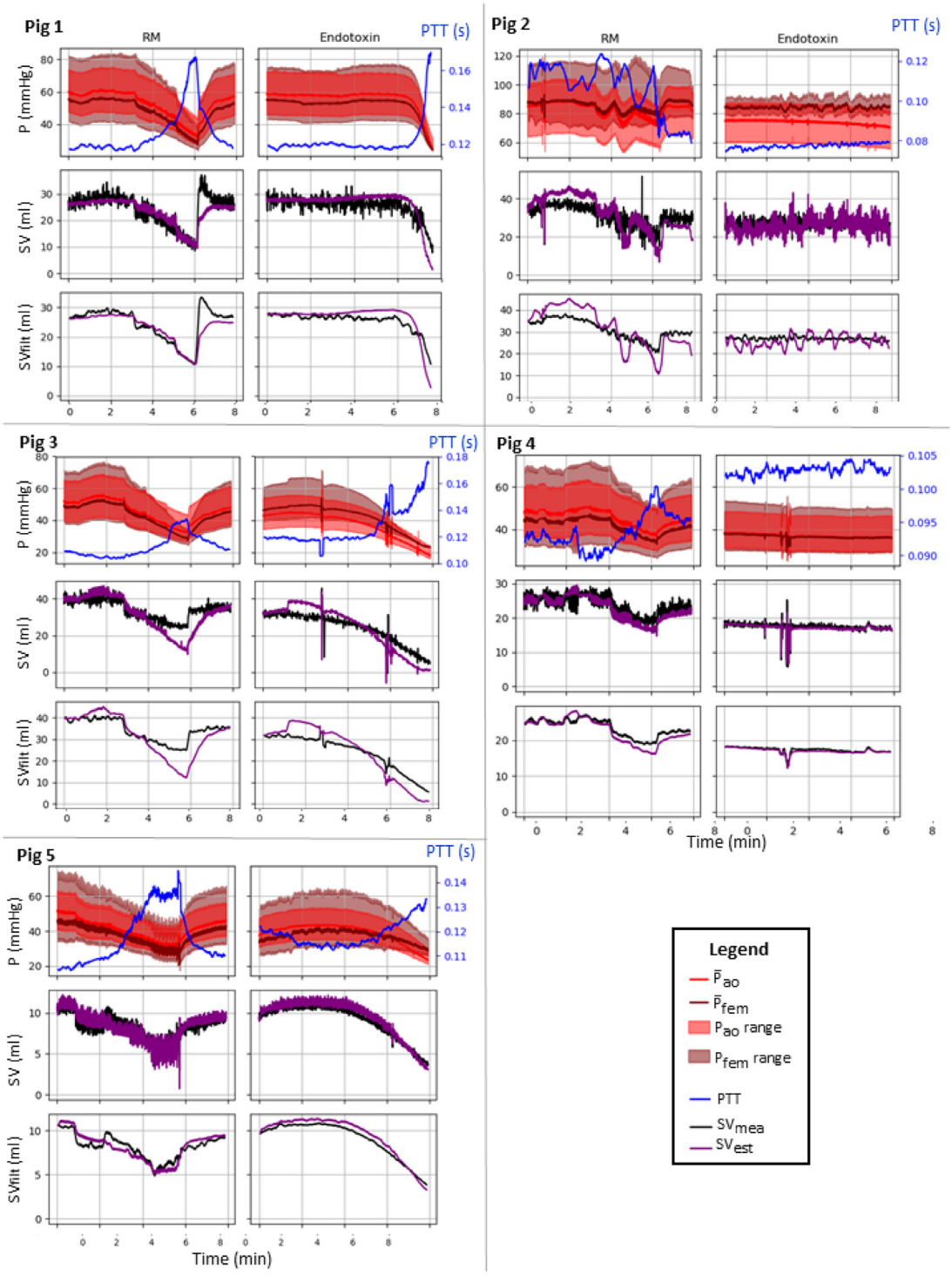

Fig. 7. Pressures, PTT, and SV for dynamic events for each pig. Beat-wise mean pressures are plotted as a line, with the range (foot-peak) shaded.

failure in Pigs 1, 3, and 5, where SV reduced to less than half its baseline value (SVs shown in Figs 6), examples of very severe hemodynamic instability.

4.2. Stroke volume estimation performance

Bland-Altman median bias and limits of agreement (2.5th, 97.5th percentile) were -10% [-49, 36] for state-change events, and -1% [-28, 20] for dynamic events (Fig 4). Thus, errors are within the acceptable range of ±30% [27] for dynamic events. For state-change events, 4 of 20 errors are outside these limits (Fig 4), all of which are cases where P_{ao} mean and pulse pressure changes differ notably to those of P_{fem}. Given the severe interventions tested, the method shows promise to potentially be able to measure *SV* with acceptable agreement in a clinical setting.

The limit of angular agreement from polar plot analysis was 35.6° for state-change events and 35.2° for dynamic events (Fig 4), both falling outside the acceptable range of 30° [29]. However, all

large ΔSVs are well within the suggested 30° limits (Fig 4), and it is largely errors just outside the 10% exclusion zone contributing to the large angular limit.

4.3. Limitations

4.3.1. Experimental interventions

A controlled pig trial will vary from critically ill patients. First, while the anatomy of the porcine and human cardiovascular systems is similar, there are differences [30]. Second, the pig trial enables higher fidelity pressure catheter signals and PTT measurement than available clinically. Third, the experimental interventions tested in the pig trial, while severe, may not represent the full range of hemodynamic states seen in critically ill patients. However, a porcine trial has the benefit of allowing comprehensive model, not feasible clinically. In future, the model should be clinically validated.

4.3.2. Model assumptions

The tube-load model greatly simplifies the arterial properties, lumping their dynamic and spatially characteristics into just 4 variables. This simplification is achieved by assuming the behaviour of the large arteries can be represented by a uniform lossless tube and the peripheral arteries are describable in the frequency domain as a single pole and zero. As a result, the model may not capture all the phenomena required to accurately relate arterial pressure and flow waveforms. However, increasing model complexity to account for losses in the large arteries, and other aspects of arterial behaviour, to potentially improve SV estimation accuracy, would increase the parameter identification complexity. This model implementation is clinically identifiable, while also able to produce realistic pressure and flow waveforms (Fig 5), and provide reasonable SV estimates (Fig 4).

Parameters α, β, describing distal peripheral arterial properties, are not readily interpretable. An alternative model for the distal load describing it as resistance and capacitance (e.g [12]) could potentially shed light on changing distal arterial muscle tone. However, it would be challenging to validate whether model parameter changes correspond to actual physiological changes, and this aspect was not the focus of this study.

Assuming Z is constant assumes both Z_c, the characteristic impedance of the large arteries, and C are constant, and thus the component of Q_{ao} travelling to the femoral artery is representative of overall Q_{ao}. The first assumption is reasonable on the basis resistance of the large arteries is low compared to the distal arteries, and they are less affected by changes in vascular tone [11]. The second assumption is based on the fact P_{fem} is a relatively large artery. However, there may be changes in regional distribution of blood flow [31], which is a possible contributing factor to error. A potential example of this effect is Pig 3, for which P_{fem} PP reduced dramatically, whereas P_{ao} PP reduced to a much lesser extent, resulting in the model overestimating SV reductions (Fig 6). This issue could be mitigated by incorporating more central, or peripheral waveform measures, at the expense of complexity, practical identifiability, and clinical ease of implementation.

Finally, to identify α, β, assumptions are made about P_{ao} and Q_{ao} shapes. The assumption of 0 diastolic flow is reasonable, as the aortic valve is closed during diastole. However, this assumption may lead to poor modelling for cases of severe aortic regurgitation, which is clinically uncommon. The assumption of an exponential pressure decay during diastole is reasonable based on observed P_{ao} waveforms [11]. While aortic decay is not always perfectly exponential, the constraint generates reasonable aortic flow waveforms (e.g. Fig 5), and avoids unrealistic pressure peaks during diastole.

5. Conclusions

A clinically identifiable implementation of the tube-load model, which uses PTT and a clinically common peripheral arterial pressure signal as inputs, has been comprehensively assessed for SV estimation accuracy, for the first time, using data from pig trials. SV estimation agreement and trending performance was reasonable given the severity of the interventions. This simple yet robust method has potential to track SV within acceptable limits during hemodynamic instability in critically ill patients, provided that a sufficiently accurate estimate of PTT can be obtained.

Declaration of competing interest

The authors declare that they have no conflicts of interest for the study titled “Tube-load model: a clinically applicable pulse contour analysis method for estimation of cardiac stroke volume” submitted to Computer Methods and Programs in Biomedicine.

Appendix A. Derivation of discrete time domain transfer functions

Frequency domain transfer functions (Eqs. 2, 3) were transformed to the time domain (Eqs. 4, 5) using the following process:

The $P_{ao} - P_{fem}$ transfer function (Eq. 2) can be rearranged as:

$$P_{ao,est}(j\omega)(j\omega + B) = P_{fem}(j\omega) \left\{ \left(\frac{B+A}{2} + j\omega \right) e^{j\omega PTT} + \left(\frac{B-A}{2} \right) e^{-j\omega PTT} \right\} \tag{A.1}$$

Transforming this to the time domain by inverse Laplace transform:

$$\dot{P}_{ao,est}(t) + BP_{ao,est}(t) = \dot{P}_{fem}(t + PTT) + \frac{B+A}{2} P_{fem}(t + PTT) + \frac{B-A}{2} P_{fem}(t - PTT) \tag{A.2}$$

The time domain equation is then discretized. Discrete derivatives are calculated using Euler's method ($\dot{P}(t) \approx F_s(P[n] - P[n-1])$), where F_s is the signal sampling frequency:

$$\begin{aligned} &F_s(P_{ao,est}[n] - P_{ao,est}[n-1]) + BP_{ao,est}[n] = \\ &F_s(P_{fem}[n + PTT \cdot F_s] - P_{fem}[n + PTT \cdot F_s - 1]) \\ &+ \frac{B+A}{2} P_{fem}[n + PTT \cdot F_s] + \frac{B-A}{2} P_{fem}[n - PTT \cdot F_s] \end{aligned} \tag{A.3}$$

Rearranging for $P_{ao,est}[n]$ and substituting in new parameters defined $\alpha = \frac{F_s}{F_s + B}$ and $\beta = \frac{(B+A)/2 + F_s}{B + F_s}$ yields the discrete time transfer function as given in Eq. 4:

$$\begin{aligned} P_{ao,est}[n] = \alpha P_{ao,est}[n-1] + \beta P_{fem}[n + PTT \cdot F_s] \\ - \alpha P_{fem}[n + PTT \cdot F_s - 1] + (1 - \beta) P_{fem}[n - PTT \cdot F_s] \end{aligned} \tag{A.4}$$

The $ZQ_{ao,est} - P_{fem}$ frequency domain transfer function (Eq. 3) is very similar to the $P_{ao,est} - P_{fem}$ transfer function. Thus the $ZQ_{ao,est} - P_{fem}$ time domain transfer function (Eq. 5) can be derived in the same manner.

Appendix B. Summary Tables

The following tables summarize measured signals (P_{ao}, P_{fem}, PTT, SV_{mea}) during state-change and dynamic events respectively.

Table B.1
Summary of measured signals for each state-change event for each pig. All values are presented as median and 95% range [2.5th percentile, 97.5th percentile]. PP refers to pulse pressure. N is the number of beats.

	Intervention	N	$\overline{P}_{fem}$ mmHg	P_{fem} PP	$\overline{P}_{ao}$	P_{ao} PP	PTT s	SV_{mea} mL
Pig	Control	10	56 [55, 56]	41 [39, 41]	60 [60, 61]	27 [26, 27]	0.116 [0.112, 0.116]	27 [25, 29]
1	h PEEP	10	46 [45, 47]	35 [33, 36]	50 [49, 51]	24 [23, 25]	0.124 [0.124, 0.124]	21 [18, 22]
	h Fluids	10	54 [54, 55]	31 [30, 32]	58 [58, 58]	26 [26, 26]	0.12 [0.116, 0.12]	26 [22, 29]
	start Endo	10	52 [52, 53]	32 [31, 32]	57 [57, 58]	26 [25, 26]	0.12 [0.117, 0.124]	26 [24, 29]
	end Endo	10	41 [38, 43]	23 [19, 26]	44 [42, 47]	19 [16, 20]	0.128 [0.128, 0.132]	21 [16, 24]
Pig	Control	10	87 [87, 88]	39 [37, 39]	85 [84, 86]	35 [34, 36]	0.084 [0.084, 0.092]	34 [32, 37]
2	h PEEP	10	82 [81, 85]	44 [40, 48]	78 [77, 82]	30 [28, 34]	0.1 [0.096, 0.1]	25 [19, 30]
	h Fluids	10	87 [86, 88]	16 [14, 18]	82 [82, 83]	32 [31, 32]	0.076 [0.076, 0.08]	29 [25, 31]
	start Endo	10	89 [89, 90]	18 [16, 19]	84 [84, 85]	34 [32, 34]	0.076 [0.076, 0.08]	30 [28, 33]
	end Endo	10	83 [83, 84]	12 [11, 13]	71 [70, 72]	26 [24, 29]	0.08 [0.076, 0.08]	26 [23, 27]
Pig	Control	10	46 [46, 47]	31 [30, 32]	49 [49, 50]	25 [25, 26]	0.104 [0.104, 0.108]	39 [37, 43]
3	h PEEP	10	40 [39, 40]	23 [21, 23]	42 [41, 42]	22 [20, 22]	0.108 [0.108, 0.112]	29 [27, 31]
	h Fluids	10	51 [51, 52]	37 [35, 38]	52 [51, 52]	27 [26, 28]	0.112 [0.108, 0.112]	42 [41, 43]
	start Endo	10	40 [40, 41]	21 [20, 22]	41 [40, 42]	21 [20, 22]	0.12 [0.12, 0.124]	35 [34, 38]
	end Endo	10	25 [24, 25]	1.0 [0.7, 1.1]	21 [20, 21]	8.0 [7.5, 9.3]	0.156 [0.136, 0.171]	8.0 [6.0, 9.4]
Pig	Control	10	43 [42, 44]	35 [34, 37]	46 [46, 48]	23 [23, 24]	0.092 [0.092, 0.096]	25 [22, 28]
4	h PEEP	10	37 [37, 38]	26 [25, 28]	40 [40, 41]	20 [19, 21]	0.092 [0.092, 0.096]	19 [18, 21]
	h Fluids	10	47 [46, 47]	36 [35, 36]	47 [47, 48]	23 [22, 23]	0.096 [0.092, 0.096]	31 [30, 32]
	start Endo	10	42 [42, 43]	33 [31, 33]	44 [44, 45]	22 [21, 22]	0.096 [0.096, 0.1]	26 [25, 29]
	end Endo	10	36 [35, 36]	21 [20, 21]	36 [36, 36]	16 [16, 16]	0.104 [0.1, 0.104]	16 [16, 17]
Pig	Control	10	45 [44, 47]	35 [33, 37]	51 [50, 51]	20 [19, 21]	0.104 [0.104, 0.108]	11 [10, 11]
5	h PEEP	10	38 [38, 40]	26 [24, 28]	41 [40, 42]	17 [16, 18]	0.112 [0.108, 0.112]	8.8 [8.2, 9.9]
	h Fluids	10	40 [40, 42]	28 [27, 30]	45 [44, 45]	19 [18, 20]	0.116 [0.116, 0.12]	12 [11, 12]
	start Endo	10	39 [38, 41]	28 [26, 29]	44 [43, 44]	19 [18, 20]	0.116 [0.113, 0.12]	12 [12, 12]
	end Endo	10	33 [32, 34]	16 [15, 17]	29 [29, 30]	12 [11, 12]	0.128 [0.124, 0.128]	5.6 [5.4, 5.7]

Table B.2
Summary of measured signals for each dynamic event for each pig. All values are presented as median and 95% range [2.5th percentile, 97.5th percentile]. PP refers to pulse pressure. N is the number of beats.

	Intervention	N	$\overline{P}_{fem}$ mmHg	P_{fem} PP	$\overline{P}_{ao}$	P_{ao} PP	PTT s	SV_{mea} mL
Pig	RM Control	10	55 [53, 55]	40 [38, 40]	59 [58, 60]	26 [24, 26]	0.116 [0.116, 0.12]	26 [23, 28]
1	RM	481	50 [29, 56]	37 [15, 42]	54 [33, 60]	26 [16, 27]	0.12 [0.116, 0.168]	26 [10, 32]
	Endo Control	10	54 [54, 55]	32 [30, 32]	58 [58, 59]	26 [25, 26]	0.12 [0.116, 0.12]	28 [23, 31]
	Endotoxin	428	53 [28, 55]	32 [6.6, 34]	58 [30, 59]	26 [11, 27]	0.12 [0.116, 0.16]	26 [13, 30]
Pig	RM Control	10	87 [86, 88]	36 [34, 39]	85 [84, 86]	35 [34, 36]	0.116 [0.088, 0.12]	34 [33, 37]
2	RM	718	86 [78, 89]	40 [22, 45]	84 [71, 88]	33 [26, 37]	0.108 [0.08, 0.124]	31 [19, 38]
	Endo Control	10	84 [84, 85]	11 [11, 11]	75 [74, 75]	26 [25, 27]	0.076 [0.072, 0.076]	26 [23, 31]
	Endotoxin	680	84 [81, 86]	12 [9.9, 13]	74 [70, 75]	26 [24, 27]	0.076 [0.072, 0.08]	26 [23, 30]
Pig	RM Control	10	48 [47, 49]	32 [30, 33]	51 [50, 52]	25 [24, 26]	0.108 [0.108, 0.112]	39 [37, 43]
3	RM	603	43 [29, 52]	27 [10, 35]	45 [33, 55]	23 [16, 27]	0.108 [0.104, 0.132]	34 [24, 42]
	Endo Control	10	46 [46, 46]	21 [20, 21]	43 [42, 43]	19 [19, 19]	0.12 [0.1169, 0.12]	31 [29, 33]
	Endotoxin	550	45 [23, 49]	20 [0.7, 25]	40 [19, 44]	17 [7.5, 19]	0.12 [0.116, 0.176]	26 [5.9, 32]
Pig	RM Control	10	43 [43, 45]	35 [34, 37]	47 [47, 49]	24 [23, 23]	0.092 [0.0889, 0.0951]	24 [22, 28]
4	RM	571	42 [34, 46]	34 [22, 38]	46 [37, 50]	23 [18, 25]	0.092 [0.088, 0.1]	23 [18, 28]
	Endo Control	10	37 [37, 38]	23 [22, 23]	38 [38, 38]	17 [17, 17]	0.102 [0.1, 0.104]	18 [17, 19]
	Endotoxin	519	36 [35, 38]	21 [19, 23]	36 [36, 38]	17 [16, 17]	0.104 [0.1, 0.104]	17 [15, 18]
Pig	RM Control	10	45 [44, 46]	37 [35, 38]	51 [50, 52]	21 [20, 22]	0.104 [0.104, 0.1071]	10 [10, 11]
5	RM	590	38 [26, 45]	28 [12, 37]	41 [29, 50]	17 [11, 21]	0.112 [0.104, 0.148]	8.3 [4.5, 10]
	Endo Control	10	34 [33, 35]	27 [26, 28]	38 [37, 38]	17 [16, 16]	0.122 [0.1169, 0.1271]	9.6 [9.2, 10]
	Endotoxin	577	38 [29, 41]	29 [10, 31]	41 [24, 43]	17 [9.3, 18]	0.116 [0.112, 0.132]	10 [4.1, 11]

References

[1] D.A. Reuter, A. Kirchner, T.W. Felbinger, F.C. Weis, E. Kilger, P. Lamm, A.E. Goetz, Usefulness of left ventricular stroke volume variation to assess fluid responsiveness in patients with reduced cardiac function, Crit. Care Med. 31 (5) (2003) 1399–1404.

[2] T. Luecke, P. Pelosi, Clinical review: positive end-expiratory pressure and cardiac output., Crit. care 9 (6) (2005) 607–621.

[3] L. Busse, D.L. Davison, C. Junker, L.S. Chawla, Hemodynamic monitoring in the critical care environment., Adv. Chronic Kidney Dis. 20 (1) (2013) 21–29.

[4] J.C. Orban, Y. Walrave, N. Mongardon, B. Allaouchiche, L. Argaud, F. Aubrun, G. Barjon, J.-M. Constantin, G. Dhonneur, J. Durand-Gasselin, H. Dupont, M. Genestal, C. Goguey, P. Goutorbe, B. Guidet, H. Hyvernat, S. Jaber, J.-Y. Lefrant, Y. Mallédant, J. Morel, A. Ouattara, N. Pichon, A.-M. Guérin Robardey, M. Sirodot, A. Theissen, S. Wiramus, L. Zieleskiewicz, M. Leone, C. Ichai, AzuRea, Causes and characteristics of death in intensive care units, Anesthesiology 126 (5) (2017) 882–889.

[5] M. Cecconi, D. De Backer, M. Antonelli, R. Beale, J. Bakker, C. Hofer, R. Jaeschke, A. Mebazaa, M.R. Pinsky, J. Louis, T. Jean, L. Vincent, A. Rhodes, M. Cecconi, Á.A. Rhodes, D. De Backer, J.L. Vincent, M. Antonelli, R. Beale, J. Bakker, C. Hofer, R. Jaeschke, P. Diderot, P. Sorbonne, P. Cité, L. Aphp, M.R. Pinsky, J.L. Teboul, Consensus on circulatory shock and hemodynamic monitoring. task force of the european society of intensive care medicine, Intensive Care Med. 40 (2014) 1795–1815.

[6] J. Grensemann, Cardiac output monitoring by pulse contour analysis, the technical basics of less-Invasive techniques, Front. Med. 5 (2018) 64.

[7] Y. Mehta, D. Arora, Newer methods of cardiac output monitoring., World J. Cardiol. 6 (9) (2014) 1022–1029.

[8] T. Desaive, O. Horikawa, J.P. Ortiz, J.G. Chase, Model-based management of cardiovascular failure: where medicine and control systems converge, Annu. Rev. Control 48 (2019) 383–391.

[9] J. Balmer, C.G. Pretty, S. Davidson, T. Mehta-Wilson, T. Desaive, R. Smith, G.M. Shaw, J.G. Chase, Clinically applicable model-based method, for physiologically accurate flow waveform and stroke volume estimation, Comput. Meth. Prog. Bio. 185 (2020) 105125.

[10] K.H. Wesseling, J.R. Jansen, J.J. Settels, J.J. Schreuder, Computation of aortic flow from pressure in humans using a nonlinear, three-element model, J. Appl. Physiol. 74 (5) (1993) 2566–2573.

[11] W.W. Nichols, M.F. ORourke, C. Vlachopoulos, D.A. McDonald, Mcdonalds blood flow in arteries: Theoretical, experimental and clinical principles, Hodder Arnold, 2011.
[12] G. Zhang, J.-O. Hahn, R. Mukkamala, Tube-load model parameter estimation for monitoring arterial hemodynamics, Front. Physiol. 2 (2011) 72.
[13] J.-O. Hahn, A.T. Reisner, H.H. Asada, Blind identification of two-channel iir systems with application to central cardiovascular monitoring, J. Dyn. Syst. Meas. Control 131 (5) (2009) 051009.
[14] W. Welkowitz, Q. Cui, Y. Qi, J. Kostis, Noninvasive estimation of cardiac output, IEEE. Trans. Biomed. Eng. 38 (11) (1991) 1100–1105.
[15] J.D. Redling, M. Akay, Noninvasive cardiac output estimation: a preliminary study, Biol. Cybern. 77 (2) (1997) 111–122.
[16] J.G. Chase, J.-C. Preiser, J.L. Dickson, A. Pironet, Y.S. Chiew, C.G. Pretty, G.M. Shaw, B. Benyo, K. Moeller, S. Safaei, et al., Next-generation, personalised, model-based critical care medicine: a state-of-the art review of in silico virtual patient models, methods, and cohorts, and how to validation them, Biomed. Eng. Online 17 (1) (2018).
[17] M. Merx, C. Weber, Sepsis and the heart, Circulation 116 (7) (2007) 793–802.
[18] J. Balmer, C. Pretty, S. Davidson, T. Desaive, S. Kamoi, A. Pironet, P. Morimont, N. Janssen, B. Lambermont, G.M. Shaw, J.G. Chase, Pre-ejection period, the reason why the electrocardiogram Q-wave is an unreliable indicator of pulse wave initialization, Physiol. Meas 39 (9) (2018) 095005.
[19] J. Balmer, R. Smith, C.G. Pretty, T. Desaive, G.M. Shaw, J.G. Chase, Accurate end systole detection in dicrotic notch-less arterial pressure waveforms, J Clin Monit Comput (2020) 1–10.
[20] A. Grillo, F. Moretti, M. Rovina, C. Baldi, L. Salvi, L. Gao, F. Scalise, G. Sorropago, A. Faini, S. Millasseau, et al., Non-invasive measurement of aortic pulse wave velocity, J. Hypertens. 36 (Supplement 1) (2018) e199.
[21] G. Swamy, D. Xu, R. Mukkamala, Estimation of the aortic pressure waveform from a radial artery pressure waveform via an adaptive transfer function: feasibility demonstration in swine, 2009 Annual International Conference of the IEEE Engineering in Medicine and Biology Society (2009) 2362–2364.
[22] G. Swamy, D. Xu, N.B. Olivier, R. Mukkamala, An adaptive transfer function for deriving the aortic pressure waveform from a peripheral artery pressure waveform, Am. J. Physiol. Heart Circ. Physiol. 297 (5) (2009) H1956–63.
[23] B. Saugel, K. Kouz, A.S. Meidert, L. Schulte-Uentrop, S. Romagnoli, How to measure blood pressure using an arterial catheter: a systematic 5-step approach, Crit. Care 24 (1) (2020).
[24] A. Levitov, H.L. Frankel, M. Blaivas, A.W. Kirkpatrick, E. Su, D. Evans, D.T. Summerfield, A. Slonim, R. Breitkreutz, S. Price, et al., Guidelines for the appropriate use of bedside general and cardiac ultrasonography in the evaluation of critically ill patients part ii, Crit. Care Med. 44 (6) (2016) 1206–1227.
[25] S.S. Mahmood, M.R. Pinsky, Heart-lung interactions during mechanical ventilation: the basics, Ann. Transl. Med. 6 (18) (2018) 349.
[26] D.G. Altman, J.M. Bland, Measurement in medicine: the analysis of method comparison studies, The Statistician 32 (3) (1983) 307.
[27] L.A. Critchley, J.A. Critchley, A meta-analysis of studies using bias and precision statistics to compare cardiac output measurement techniques., J Clin Monit Comput 15 (2) (1999) 85–91.
[28] P.J. Peyton, S.W. Chong, Minimally invasive measurement of cardiac output during surgery and critical care, Anesthesiology 113 (5) (2010) 1220–1235.
[29] L.A. Critchley, X.X. Yang, A. Lee, Assessment of trending ability of cardiac output monitors by polar plot methodology, J. Cardiothorac. Vasc. Anesth. 25 (3) (2011) 536–546.
[30] P.P. Lelovas, N.G. Kostomitsopoulos, T.T. Xanthos, A comparative anatomic and physiologic overview of the porcine heart., J. Am. Assoc. Lab. Anim. Sci. 53 (5) (2014) 432–438.
[31] M.R. Pinsky, Regional blood flow distribution, Update in Intensive Care and Emergency Medicine The Splanchnic Circulation (1995) 1–13.